Probing the Structures and Lanthanum-Lanthanum Bonding in $La_2B_{n}^-$ (n = 4-6) Clusters

Jordan Burkhardt^{1#}, Teng-Teng Chen^{2,4#}*, Wei-Jia Chen³, Dao-Fu Yuan^{3,5}, Wan-Lu Li^{1,6}*, and Lai-Sheng Wang³*

ABSTRACT: We report an investigation on the structures and chemical bonding in a series of dilanthanum boron clusters, $La_2B_n^-(n=4-6)$, using photoelectron spectroscopy and theoretical calculations. Well-resolved photoelectron spectra are obtained and used to verify the global minima of the lanthanide boron clusters. The structures of $La_2B_4^-$ and $La_2B_5^-$ are found to consist of open B_4 and B_5 rings, respectively, around the La_2 dimer equatorially. Theoretical evidence of La-La σ bonding is obtained in $La_2B_4^-$, whereas the bonding in $La_2B_5^-$ is similar to an incomplete inverse sandwich without real La-La bonding. The global minimum of $La_2B_6^-$ is completely different, where one of the La atoms can be viewed as substituting a B atom of the B_7 cluster due to the high electronic stability of the B_7^{3-} borozene. The resulting lanthaborozene $[LaB_6]^{3-}$ forms a half-sandwich structure with the second La atom with evidence of La-La σ bonding. Lanthanide-lanthanide bonds are relatively rare in chemistry. The current work suggests that binary lanthanide boron clusters provide interesting systems to study lanthanide-lanthanide bonding.

¹Aiiso Yufeng Li Family Department of Chemical and Nano Engineering, University of California San Diego, CA 92093, USA

²Department of Chemistry, The Hong Kong University of Science and Technology, Clear Water Bay, Kowloon, Hong Kong (SAR) 999077 (China)

³Department of Chemistry, Brown University, Providence, Rhode Island 02912, USA

⁴HKUST Shenzhen-Hong Kong Collaborative Innovation Research Institute, Shenzhen 518045, China

⁵Hefei National Research Center for Physical Science at Microscale, University of Science and Technology of China, Hefei 230026, China

⁶Program in Materials Science and Engineering, University of California San Diego, CA 92093, USA

1. INTRODUCTION

Metal-metal bonding is well known in the chemistry of transition metals, but rare for the lanthanide (Ln). Ln–Ln covalent bonding was first observed in endohedral Ln₂ dimers encapsulated in fullerene cages. ¹⁻⁶ In these metallofullerene molecules, both single-electron and two-electron Ln–Ln σ bonds have been observed, depending on the degree of charge transfer from the Ln atoms to the fullerene cage. Outside the confined environment of the fullerenes, the first single-electron Ln–Ln σ bond was recently observed in the $(Cp^{iPr5})_2Ln_2I_3$ complexes (Ln = Y, Gd, Tb, Dy; Cp^{iPr5} = pentaisopropylcyclopentadienyl), where the two lanthanide atoms are bridged by three I atoms and each coordinated axially by a Cp^{iPr5} ligand. ⁷ The mixed-valence Ln–Ln bond comes from the σ molecular orbital (MO) of $5d_z^2$ parentage, occupied by a single electron. Thus, the oxidation state of each Ln atom is formally +2.5. Ln–Ln bonding was not observed in the $(Cp^{iPr5})_2Ln_2I_4$ precursor because each Ln atom is in their favorite +3 oxidation state.

Ln-Ln bonding should exist in Ln clusters and has been studied in the La₃⁻ cluster⁸ and other lanthanide suboxide clusters, 9,10 which were investigated using photoelectron spectroscopy (PES) and theoretical calculations. We have recently investigated a series of di-lanthanum boron clusters, $La_2B_n^-$ (n = 7–11), using PES and quantum chemistry and found that they all possess inverse-sandwich structures consisting of B_n monocyclic rings. ¹¹⁻¹⁴ In addition to aromatic stabilization in the B_n ring, these complexes are stabilized by multi-center δ bonding between the π orbitals of the B_n rings and the 5d orbitals of the La atoms. Even though the La-La distance was found to be relatively short in the inverse-sandwich complexes, no La-La covalent bond was found because all the valence electrons of the La atoms are used to form bonds with the B_n ring. An interesting question is if La–La covalent bonding may exist in smaller $La_2B_n^-$ clusters with $n \le 6$. There have been relatively few studies on lanthanide-doped boron clusters, ¹⁵-²² mostly focusing on mono-Ln doped boron clusters. We have also studied several larger B-rich Ln₃B_n clusters, 23,24 including the inverse triple decker La_3B_{14} cluster and the Ln_3B_{18} (Ln = La, Tb) spherical trihedral metallo-borospherenes, which do not contain Ln-Ln bonding. Understanding the Ln-Ln and Ln-B bonding in small clusters is not only important in their own right, it may also provide insight into the electronic structure and chemical bonding of bulk lanthanide borides, 25 which are a class of technologically important materials. 26-28

Here we report a joint PES and theoretical investigation of di-lanthanum boron clusters, $La_2B_n^-$ (n = 4-6) and the observation of La–La σ bonding of 6s/5d characters. The global minima of $La_2B_4^-$ and $La_2B_5^-$ are found to consist of open B_4 and B_5 rings, respectively, around a La_2 dimer equatorially. A single-electron σ bond is observed in $La_2B_4^-$, whereas no direct La–La bond is found in $La_2B_5^-$. The global

minimum structure of $La_2B_6^-$ contains two different types of La atoms. One of the La atoms can be viewed as substituting a B atom of the C_{6v} B_7 cluster due to the electronic stability of the B_7^{3-} borozene. The resulting lanthaborozene $[LaB_6]^{3-}$ then forms a half-sandwich with the second La atom and a single-electron La-La σ bond at the same time. The single-electron La-La σ bonds in $La_2B_4^-$ and $La_2B_6^-$ are of 6s/5d characters and are analogous to the single-electron Ln-Ln bond in the metallofullerenes and the $(Cp^{iPr5})_2Ln_2I_3$ complexes.

2. EXPERIMENTAL AND THEORETICAL METHODS

- **2.1. Photoelectron Spectroscopy.** The experiments were conducted using a magnetic-bottle PES apparatus, along with a laser vaporization cluster source and a time-of-flight mass spectrometer. Detailed information about the experimental apparatus and procedure has been published previously.³⁰ Briefly, the lanthanide boride clusters were generated by laser vaporization of a disc target made from a mixed powder of La (Alfa Aesar, 99.9% purity) and B (Alfa Aesar, 96% ¹¹B-enriched, 99.9% elemental purity) with a 5/2 La/B mass ratio. The resulting laser-induced plasma was quenched by a helium carrier gas mixed with 5% argon inside the nozzle, which initiated cluster formation. The nascent clusters were entrained by the carrier gas and underwent a supersonic expansion to create a cold cluster beam. After passing through a skimmer, negatively charged clusters were extracted from the collimated beam and analyzed using a timeof-flight mass spectrometer. A series of La_xB_y clusters were formed in the source and the cluster distribution can be optimized to some degree, i.e., the relative ratios of the La/B in the target and the resident time of the clusters in the nozzle. The clusters of current interest, La₂B_n $^-$ (n = 4-6), were each mass-selected, and decelerated before being photodetached by the 193 nm radiation from an ArF excimer laser. As discussed previously, ³⁰ the temperature of the clusters depended on their resident time inside the nozzle. To ensure colder clusters, we typically chose those with the longest resident time. Photoelectrons were collected at nearly 100% efficiency by the magnetic bottle and analyzed in a 3.5 m long electron flight tube. Photoelectron spectra were calibrated using the known spectrum of the Bi⁻ atomic anion. The PES apparatus provided an electron kinetic energy (KE) resolution ($\Delta KE/KE$) of around 2.5%, that is, ~25 meV for 1 eV electrons.
- **2.2. Computational Methods.** We used a new global minimum search algorithm SDGMS developed in the Li group at UCSD to search for the global minima of the La₂B_n⁻ (n = 4-6) clusters.³¹ The algorithm begins with a starting structure selected from the top of a stack, which is then explored in 6n directions corresponding to the $\pm x$, $\pm y$, and $\pm z$ coordinates for each atom. Each atom is displaced by a user-defined

distance (0.2 Å in this study) in these directions. If the new structure does not violate covalent bonding requirements, an *ab initio* energy calculation is performed. This iterative process continues until the energy decreases, indicating the escape from the potential well, or until a predefined number of uphill steps is reached (20 steps in this study). Upon escaping the potential well, a geometry optimization is performed, and the new structure is added to the stack if it is unique from all previously optimized structures within a specified distance (0.2 Å). The algorithm employs a stack data structure to enable a depth-first search approach. Atomic distances are estimated heuristically, and the stack of structures is initialized via a seed generation algorithm that utilizes point group symmetries. Although each structure can theoretically be explored in infinite directions, all possible directions can be represented as combinations of vectors in the x, y, and z directions, assuming the vector size is infinitesimal. Consequently, reducing the exploration to 6n directions per structure significantly narrows the search space without missing any local minima, provided the step size is sufficiently small. Furthermore, structure similarity searching and covalent criteria filtering at each step reduce the search space. The energies of different structures were calculated using ADF, 32,33 with the zero-order regular approximation (ZORA), 34 the TZP basis set with large frozen cores, 35 and the PBE exchange-correlation functional.

The adiabatic detachment energy (ADE) was computed for the global minimum using the energy difference between the anionic and neutral species, each at their optimized geometries (Table 1). Single-point calculations at the DLPNO-CCSD(T) level were performed using the Def2-TZVP basis sets for the first vertical detachment energy (VDE1) and the ADE of the global minima, implemented in the ORCA software.^{37,38} Higher VDEs were obtained using the ΔSCF-TDDFT approach³⁹ using the SAOP exchange-correlation functional⁴⁰ at the TZP level without frozen cores, to compare with the experimental PES data. Chemical bonding was analyzed using both the MOs and the AdNDP method,⁴¹ carried out in Gaussian 16⁴² using the PBE functional, the ECP28MWB pseudopotential for La,^{43,44} along with the ECPMWB_SEG basis set and the cc-pVTZ basis set.⁴⁵⁻⁴⁷ The energy decomposition analysis with natural orbitals for chemical valence method (EDA-NOCV)^{48,49} was conducted using the PBE0 functional with the TZP basis set, a small frozen core, and ZORA to analyze the contributions of La and boron fragments towards the MOs.

3. RESULTS

3.1. Photoelectron Spectroscopy. The photoelectron spectra of $La_2B_n^-$ (n = 4-6) at 193 nm are depicted in Figure 1 (top row), along with the simulated spectrum for the global minimum of each cluster

(bottom row). The PES bands are labeled with letters (X, A, B, ...) and the VDEs measured from the maxima of each band for $La_2B_n^-$ (n = 4-6) are presented in Tables 2-4, respectively, where they are compared with the theoretical results.

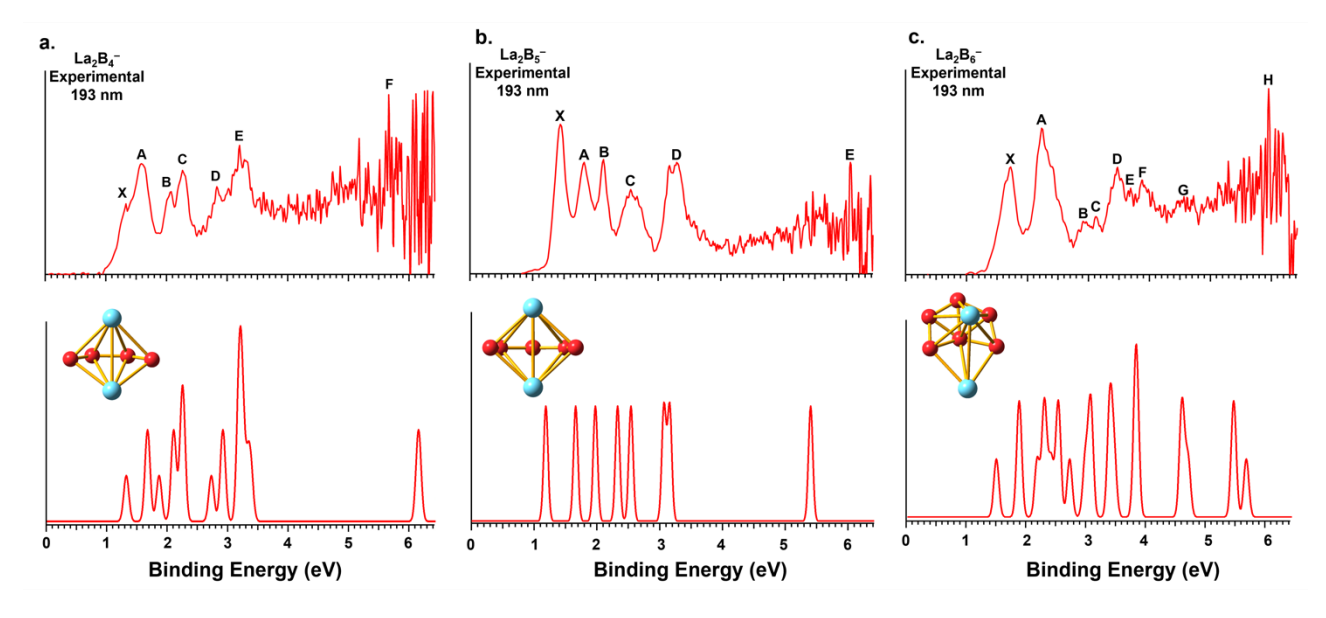


Figure 1. Photoelectron spectra of (a) La₂B₄⁻, (b) La₂B₅⁻, and (c) La₂B₆⁻, at 193 nm (6.424 eV) (top) and the simulated spectra (bottom) for the global minimum structures. A unit-area Gaussian function of 0.08 eV half-width was used for each detachment channel to generate the simulated spectra. A 2-to-1 ratio was used for triplet and singlet final states.

The spectrum of La₂B₄⁻ displays six detachment bands in the lower binding energy region, labeled as X–E (Figure 1a, top). The lowest binding energy band (X) gives rise to the VDE1 at 1.33 eV. The ADE is estimated from the onset of band X as 1.21 eV, which is also the electron affinity (EA) of the corresponding neutral La₂B₄. An overlapping band A is observed at a VDE of 1.59 eV, followed by two well- resolved bands B and C at 2.08 and 2.26 eV, respectively. A weaker band D is observed at 2.83 eV, followed by a prominent band E at 3.21 eV. Beyond 5 eV, the signal-to-noise ratio deteriorates, and a band F at ~5.7 eV is tentatively labeled for the sake of discussion. The spectrum of La₂B₄⁻ exhibits relatively complex features, due to its open-shell nature (*vide infra*).

The spectrum of La₂B₅⁻ exhibits relatively simpler patterns with five well-resolved bands in the low binding energy region (Figure 1b top), indicating it is likely a closed-shell system (*vide infra*). The lowest binding energy band X gives rise to a VDE1 of 1.44 eV, and an estimated ADE of 1.35 eV, i.e. the EA for La₂B₅. Two sharp and well-resolved bands A and B are observed at VDEs of 1.82 eV and 2.13 eV, respectively. Two broader bands C and D are observed at 2.56 eV and 3.30 eV, respectively. Above 5 eV, the signal-to-noise ratio becomes poor and no major spectral transitions are observed; a band E at ~6 eV is tentatively labeled for the sake of discussion.

The spectrum of La₂B₆⁻ (Figure 1c top) again displays relatively congested spectral patterns, indicating an open-shell system (*vide infra*). The lowest binding energy band X yields the VDE1 at 1.73 eV, but its large spectral width suggests the possible presence of multiple detachment channels, i.e., the VDE1 may represent an average value. The ADE, i.e. the EA of neutral La₂B₆, is estimated from its onset at 1.46 eV. An intense and broad band A is observed at a VDE of 2.23 eV, followed by two weak and overlapping bands B and C at VDEs of 2.91 and 3.12 eV, respectively. Three close-lying broad bands D, E, and F are observed at 3.48, 3.69, and 3.88 eV, respectively, followed by a broad band G at 4.57 eV. Beyond 5 eV, the signal-to-noise ratio deteriorates, and a band H at ~6 eV is tentatively labeled for the sake of discussion.

3.2. Global Minimum Structure Searches. The optimized global minimum structures for La₂B_n⁻ (n = 4-6) at the PBE/TZP level are depicted in Figure 2 and their coordinates are given in Table S1. Low-lying isomers for each cluster within about 1 eV of the global minimum structure are presented in Figures S1–S3 for La₂B_n⁻ (n = 4-6), respectively. For La₂B₄⁻, the SDGMS global minimum search resulted in 41 local minima. The global minimum is found to be open-shell (2 A') with C_s symmetry (Figure 2), all other structures being significantly higher in energy (Figure S1). This structure may be viewed as an incomplete inverse sandwich configuration with an open B₄ ring built around the two La atoms. The SDGMS global minimum search for La₂B₅⁻ generated a total of 236 local minima. The closed-shell structure (1 A₁) with C_{2v} symmetry was identified as the global minimum (Figure 2), while all other structures were found to have higher energies (Figure S2). Similar to La₂B₄⁻, the C_{2v} structure of La₂B₅⁻ also features an incomplete inverse sandwich arrangement with an open B₅ ring.

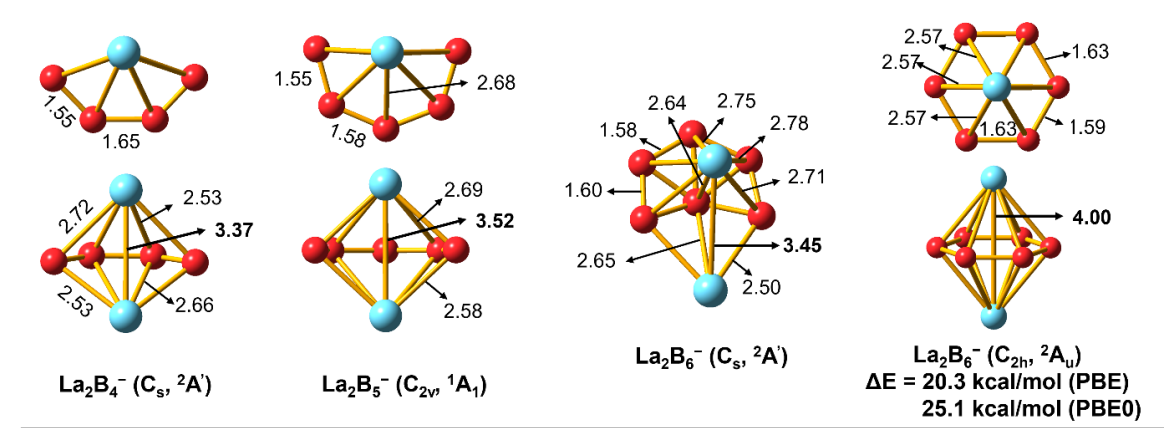


Figure 2. The optimized global minimum structures of $La_2B_4^-$ (C_s , $^2A'$), $La_2B_5^-$ (C_{2v} , 1A_1), and $La_2B_6^-$ (C_s , $^2A'$) at the PBE/TZP level. The bond lenghts are given in Å and the La–La distances are highlighted in bold. For $La_2B_6^-$, the inverse sandwich cluster (C_{2h} , 2A_u) is included for comparison.

The SDGMS global minimum search for La₂B₆⁻ resulted in more than 200 local minima. The open-shell structure (²A') with C_s symmetry was identified as the global minimum, overwhelmingly more stable

than any other isomers (Figure S3). The expected inverse sandwich cluster consisting of a monocyclic B_6 ring (C_{2h} , 2A_u) is included in Figure 2 for comparison. However, this high symmetry structure was found to be energetically unfavorable, being 20.3 kcal/mol higher in energy than the global minimum at the PBE/TZ2P level and 25.1 kcal/mol higher at the PBE0/TZP level (Figure 2 and Figure S3). It is noteworthy that the global minimum structure of the $La_2B_6^-$ cluster departs from the growth path toward the inverse-sandwich. Instead, the global minimum of $La_2B_6^-$ contains two types of La atoms. One of the La atoms seems to substitute a B atom of a B_7 cluster, 50 which then forms a half sandwich with the second La atom. Such substitutional B_7 -like structures were first observed in the AlB_6^- cluster 51 and also in lanthanide-doped LnB_6^- clusters, 16,18 as well as other main group 52 and transition metal doped MB_6^- clusters, $^{53-55}$ as a result of the high electronic stability of the B_7^{3-} borozene. 19,29

The structural evolution of La₂B_n⁻ (n = 4-6) is reminiscent of that found in Ta₂B_n⁻ (n = 4-6) previously, ^{56,57} except that the global minimum of Ta₂B₆⁻ is a perfect inverse sandwich (D_{6h}) due to the strong d-p-d bonding between the B₆ ring and the two Ta atoms. ⁵⁷ The current results are also consistent with our previous conclusion that the smallest monocyclic B_n ring to form the inverse sandwich Ln₂B_n⁻ structures is B₇. ¹¹⁻¹⁴ Interestingly, the La–La distances calculated for the global minima of La₂B_n⁻ (n = 4-6) are 3.37 Å, 3.52 Å, and 3.45 Å, respectively (Figure 2), which are all shorter than the La–La single bond length of 3.60 Å, according to Pyykkö's atomic covalent radii. ⁵⁸ These La–La bond distances are also shorter than the recently reported Ln–Ln distance in the (Cp^{iPr5})₂Ln₂I₃ compound. ⁷ MO analyses presented in Table S2 indicate that the La–La σ bonding arises from the hybridized 6s/5d orbitals of the La atoms (*vide infra*).

4. DISCUSSION

4.1. Comparison between Experiment and Theory. The VDE1 and ADE values computed for the global minimum structures of the three $La_2B_n^-$ clusters at three levels of theory are compared with the experimental values in Table 1. The simulated spectra are compared with the experimental data in Figure 1. In the case of $La_2B_4^-$ and $La_2B_6^-$, the first detachment channel corresponds to the removal of the singly occupied HOMO, i.e., 46a' for $La_2B_4^-$ (Table 2) and 50a' for $La_2B_6^-$ (Table 4). These orbitals mainly involve La-La σ bonding primarily from the hybridized 6s/5d atomic orbitals, as illustrated in Table S2. The three methods give similar and consistent ADE and VDE1 values, with the computed values slightly underestimated relative to the experimental data. The calculated VDE1 values are 1.31 eV for $La_2B_4^-$ and 1.55 eV for $La_2B_6^-$ at DLPNO-CCSD(T), which agree well with the experimental values of 1.33 eV and

Table 1. Comparison of the experimental ADE and VDE1 of La_2B_n^- (n = 4-6) with theoretical values calculated for the global minima (Figure 2) at the levels of PBE/TZP, PBE0/TZP, and single-point DLPNO-CCSD(T) methods.

	ADE (eV)					VDE1 (eV)		
	Exp ^a	PBE	PBE0	DLPNO-CCSD(T)	Exp ^b	PBE	PBE0	DLPNO-CCSD(T)
$La_2B_4^-$	1.21	1.03	1.01	0.97	1.33	1.31	1.31	1.31
$\mathrm{La_2B_5}^-$	1.35	1.10	1.23	1.18	1.44	1.22	1.23	1.34
$La_2B_6^-$	1.46	1.26	1.31	1.27	1.73	1.48	1.49	1.55

^aExperimental uncertainty: ±0.08 eV. ^bExperimental uncertainty: ±0.05 eV.

Table 2. VDEs of $La_2B_4^-$ measured from the photoelectron spectrum and compared with computed VDEs at the SAOP/TZP level for the global minimum structure of $La_2B_4^-$ (Figure 2). All energies are in eV.

Feature	VDE (exp) ^a	State	Final-state Electron Configuration	VDE (theo)
X	1.33	¹ A'	$(42a')^2(43a')^2(44a')^2(20a'')^2(45a')^2(21a'')^2(22a'')^2$ (46a') ⁰	1.31
A	1.59	³ A''	$(42a')^2(43a')^2(44a')^2(20a'')^2(45a')^2(21a'')^2$ (22a'') ¹ (46a') ¹	1.66
		¹ A''	$(42a')^2(43a')^2(44a')^2(20a'')^2(45a')^2(21a'')^2$ (22a'') ¹ (46a') ¹	1.85
В	2.08	³ A''	$(42a')^2(43a')^2(44a')^2(20a'')^2(45a')^2(21a'')^1(22a'')^2(46a')^1$	2.09
C	2.26	¹ A''	$(42a')^2(43a')^2(44a')^2(20a'')^2(45a')^2(21a'')^1(22a'')^2(46a')^1$	2.23
		³ A'	$(42a')^2(43a')^2(44a')^2(20a'')^2$ $(45a')^1(21a'')^2(22a'')^2(46a')^1$	2.24
D	2.83	¹ A'	$(42a')^2(43a')^2(44a')^2(20a'')^2$ $(45a')^1(21a'')^2(22a'')^2(46a')^1$	2.71
		³ A''	$(42a')^2(43a')^2(44a')^2(20a'')^1(45a')^2(21a'')^2(22a'')^2(46a')^1$	2.90
E	3.21	¹ A''	$(42a')^2(43a')^2(44a')^2(20a'')^1(45a')^2(21a'')^2(22a'')^2(46a')^1$	3.17
		³ A'	$(42a')^2(43a')^2(44a')^1(20a'')^2(45a')^2(21a'')^2(22a'')^2(46a')^1$	3.17
		³ A'	$(42a')^2$ $(43a')^1$ $(44a')^2$ $(20a'')^2$ $(45a')^2$ $(21a'')^2$ $(22a'')^2$ $(46a')^1$	3.22
		¹ A'	$(42a')^2(43a')^2(44a')^1(20a'')^2(45a')^2(21a'')^2(22a'')^2(46a')^1$	3.31
		¹ A'	$(42a')^2$ $(43a')^1$ $(44a')^2$ $(20a'')^2$ $(45a')^2$ $(21a'')^2$ $(22a'')^2$ $(46a')^1$	3.36
F	~5.7	³ A'	$(42a')^{1}(43a')^{2}(44a')^{2}(20a'')^{2}(45a')^{2}(21a'')^{2}(22a'')^{2}(46a')^{1}$	6.12

^aExperimental uncertainty: ±0.05 eV.

1.73 eV, respectively (Table 1). For La₂B₅⁻, the first detachment channel comes from electron removal from the 5b₁ orbital (Table 3), which involves La–B bonding through d-p δ interaction (Table S2). The

calculated VDE1 value of 1.34 eV at DLPNO-CCSD(T) is in good accord with the experimental value of 1.44 eV (Table 1).

Higher VDEs were computed using the ΔSCF-TDDFT method,³⁹ as compared with the experimental results in Tables 2–4 for La₂B_n⁻ (n = 4-6), respectively. Because La₂B₄⁻ and La₂B₄⁻ are open shell with an unpaired electron in the HOMO, both singlet and triplet final states are possible. In the case of La₂B₄⁻, band A corresponds to two final spin states (³A" and ¹A") due to electron detachment from the fully occupied 22a" orbital. This orbital consists of interactions between La₂ (d π _u) and B₄ (π ₁), as depicted in Figure 3 and Table S2. Band B, with a calculated VDE of 2.09 eV, corresponds to the ³A" final state due to electron detachment from the 21a" MO, which involves interactions between La₂ (d π _g) and B₄ (π ₁). EDA-NOCV analyses, as presented in Table S3, indicate that the 22a" and 21a" orbitals contribute significantly to the total orbital interaction energy (ΔE_{orb}), with the 22a" orbital contributing 45% and the 21a" orbital contributing 31%. Higher detachment channels C and D arise from the B₄-dominated orbitals 45a' and 20a", respectively. Band E contains contributions from multiple detachment channels, primarily from the B₄-dominated 44a' and 43a' orbitals. These orbitals have relatively small contributions to the ΔE_{orb} , as given in Table S3 (only 2.7% from 44a'). The high binding energy signals around F likely come from the 42a' MO, which is almost a pure σ orbital on the B₄ motif (92%), as shown in Table S2.

Table 3. VDEs of $La_2B_5^-$ measured from the photoelectron spectrum and compared with the computed VDEs at the SAOP/TZP level for the global minimum structure of $La_2B_5^-$ (Figure 2). All energies are in eV.

Feature	VDE (exp) ^a	State	Final-state Electron Configuration	VDE (theo)
X	1.44	$^{2}\mathrm{B}_{1}$	$3b_2^26a_1^24b_1^27a_1^24b_2^22a_2^25b_2^2$ 5b ₁ ¹	1.23
A	1.82	$^{2}\mathrm{B}_{2}$	$3{{b_{2}}^{2}}6{{a_{1}}^{2}}4{{b_{1}}^{2}}7{{a_{1}}^{2}}4{{b_{2}}^{2}}2{{a_{2}}^{2}}5{{b_{2}}^{1}}5{{b_{1}}^{2}}$	1.70
В	2.13	$^{2}A_{2}$	$3{{b_{2}}^{2}}6{{a_{1}}^{2}}4{{b_{1}}^{2}}7{{a_{1}}^{2}}4{{b_{2}}^{2}}2{{a_{2}}^{1}}5{{b_{2}}^{2}}5{{b_{1}}^{2}}$	2.01
C	2.56	$^{2}\mathrm{B}_{2}$	$3{{b_{2}}^{2}}6{{a_{1}}^{2}}4{{b_{1}}^{2}}7{{a_{1}}^{2}}4{{b_{2}}^{1}}2{{a_{2}}^{2}}5{{b_{2}}^{1}}5{{b_{1}}^{2}}$	2.36
		$^{2}A_{1}$	$3b_2^26a_1^24b_1^2\mathbf{7a_1}^14b_2^22a_2^25b_2^15b_1^2$	2.57
D	3.30	$^{2}\mathrm{B}_{1}$	$3b_2^26a_1^2\mathbf{4b_1}^17a_1^24b_2^22a_2^25b_2^15b_1^2$	3.09
		$^{2}A_{1}$	$3b_2^2$ 6a₁¹ $4b_1^2$ 7a ₁ ¹ $4b_2^2$ 2a ₂ ² $5b_2^1$ 5b ₁ ²	3.18
Е	~6.1	$^{2}\mathrm{B}_{2}$	$\mathbf{3b_2}^{1} 6 {a_1}^2 4 {b_1}^2 7 {a_1}^{1} 4 {b_2}^2 2 {a_2}^2 5 {b_2}^{1} 5 {b_1}^2$	5.40

^aExperimental uncertainty: ±0.05 eV.

Unlike in La₂B₄⁻, there is no occupied La–La σ bonding orbital in La₂B₅⁻, because the corresponding orbital (8a₁) is unoccupied, as shown in Table S2. Since La₂B₅⁻ is closed-shell, detachment from each

occupied MO leads to one PES peak, which is responsible for its relatively simple photoelectron spectrum (Figure 1b). Peaks A and B in Figure 1b correspond to the La–B bonding orbitals 5b₂ and 2a₂, respectively. The broader bands C and D each result from two close detachment channels: 4b₂ and 7a₁ for band C and 4b₁ and 6a₁ for band D (Table 3). The computed VDE for detachment from the B₅-domianted 3b₂ MO (Table S2) is 5.4 eV, which is consistent with the weak signals beyond 5 eV in the photoelectron spectrum (Figure 1b).

Table 4. VDEs of La₂B₆⁻ measured from the photoelectron spectrum and compared with the computed VDEs at the SAOP/TZP level for the global minimum structure of La₂B₆⁻ (Figure 2). All energies are in eV.

Feature	VDE (exp.) ^a	State	Configuration	VDE (theo.)
X	1.73	¹ A'	$(45a')^2(46a')^2(47a')^2(21a'')^2(22a'')^2(48a')^2(23a'')^2(49a')^2$	1.48
		³ A'	$(45a')^2(46a')^2(47a')^2(21a'')^2(22a'')^2(48a')^2(23a'')^2$ (49a') ¹ (50a') ¹	1.86
A	2.23	¹ A'	$(45a')^2(46a')^2(47a')^2(21a'')^2(22a'')^2(48a')^2(23a'')^2$ (49a') ¹ (50a') ¹	2.16
		³ A''	$(45a')^2(46a')^2(47a')^2(21a'')^2(22a'')^2(48a')^2$ (23a'') ¹ $(49a')^2(50a')^1$	2.28
		¹ A''	$(45a')^2(46a')^2(47a')^2(21a'')^2(22a'')^2(48a')^2$ (23a'') ¹ $(49a')^2(50a')^1$	2.39
		³ A'	$(45a')^2(46a')^2(47a')^2(21a'')^2(22a'')^2$ $(48a')^1(23a'')^2(49a')^2(50a')^1$	2.51
В	2.91	¹ A'	$(45a')^2(46a')^2(47a')^2(21a'')^2(22a'')^2$ $(48a')^1(23a'')^2(49a')^2(50a')^1$	2.70
		¹ A''	$(45a')^2(46a')^2(47a')^2(21a'')^2$ $(22a'')^1(48a')^2(23a'')^2(49a')^2(50a')^1$	2.96
C	3.12	³ A''	$(45a')^2(46a')^2(47a')^2(21a'')^2$ $(22a'')^1(48a')^2(23a'')^2(49a')^2(50a')^1$	3.05
D	3.48	³ A''	$(45a')^2(46a')^2(47a')^2(21a'')^1(22a'')^2(48a')^2(23a'')^2(49a')^2(50a')^1$	3.37
		¹ A''	$(45a')^2(46a')^2(47a')^2(21a'')^1(22a'')^2(48a')^2(23a'')^2(49a')^2(50a')^1$	3.44
Е	3.69	¹ A'	$(45a')^2(46a')^2(47a')^1(21a'')^2(22a'')^2(48a')^2(23a'')^2(49a')^2(50a')^1$	3.80
F	3.88	³ A'	$(45a')^2(46a')^2(47a')^1(21a'')^2(22a'')^2(48a')^2(23a'')^2(49a')^2(50a')^1$	3.81
G	4.57	³ A'	$(45a')^2$ $(46a')^1$ $(47a')^2$ $(21a'')^2$ $(22a'')^2$ $(48a')^2$ $(23a'')^2$ $(49a')^2$ $(50a')^1$	4.57
		¹ A'	$(45a')^2$ $(46a')^1$ $(47a')^2$ $(21a'')^2$ $(22a'')^2$ $(48a')^2$ $(23a'')^2$ $(49a')^2$ $(50a')^1$	4.67
Н	~6.0	³ A'	$(45a')^{1}(46a')^{2}(47a')^{2}(21a'')^{2}(22a'')^{2}(48a')^{2}(23a'')^{2}(49a')^{2}(50a')^{1}$	5.43
		¹ A'	$(45a')^{1}(46a')^{2}(47a')^{2}(21a'')^{2}(22a'')^{2}(48a')^{2}(23a'')^{2}(49a')^{2}(50a')^{1}$	5.64

^aExperimental uncertainty: ±0.05 eV.

Because La₂B₆⁻ is open shell like La₂B₄⁻, both singlet and triplet final states are possible, giving rise to a more congested spectrum (Figure 1c). Several PES bands in Figure 1c correspond to multiple

detachment channels, as shown in Table 4. In fact, the first PES band X contains two detachment channels: the detachment from the 50a' HOMO leading to the 1 A' ground state of La₂B₆ (computed VDE at 1.48 eV) and the detachment from the 49a' HOMO-1 leading to the 3 A' excited state (computed VDE at 1.86 eV). The singly occupied HOMO involves La–La d/s σ bonding, whereas the 49a' HOMO-1 is a La–B π bonding orbital (57% La $d\pi$), as shown in Table S2. The relatively small energy gap between the HOMO and HOMO-1 of La₂B₆-, which also corresponds to the LUMO-HOMO gap of neutral La₂B₆, suggests that the La–La bonding is important in the La₂B₆- cluster. The intense and broad band A contains four detachment channels: the 1 A' final state from the 49a' MO, the 3 A" and 1 A" final states from the 23a" MO, and the 3 A' final state from the 48a' MO. The computed VDEs for the higher detachment channels are all in good agreement with the congested spectral features (Table 4), including the weak signals beyond 5 eV (around H), which correspond to detachment from the B₆-based 45a' MO (95% B 2s/2p, see Table S2).

The good agreement between the experimental data and the computed ADE and VDEs for all the $La_2B_n^-$ (n = 4-6) clusters validates their global minimum structures shown in Figure 2.

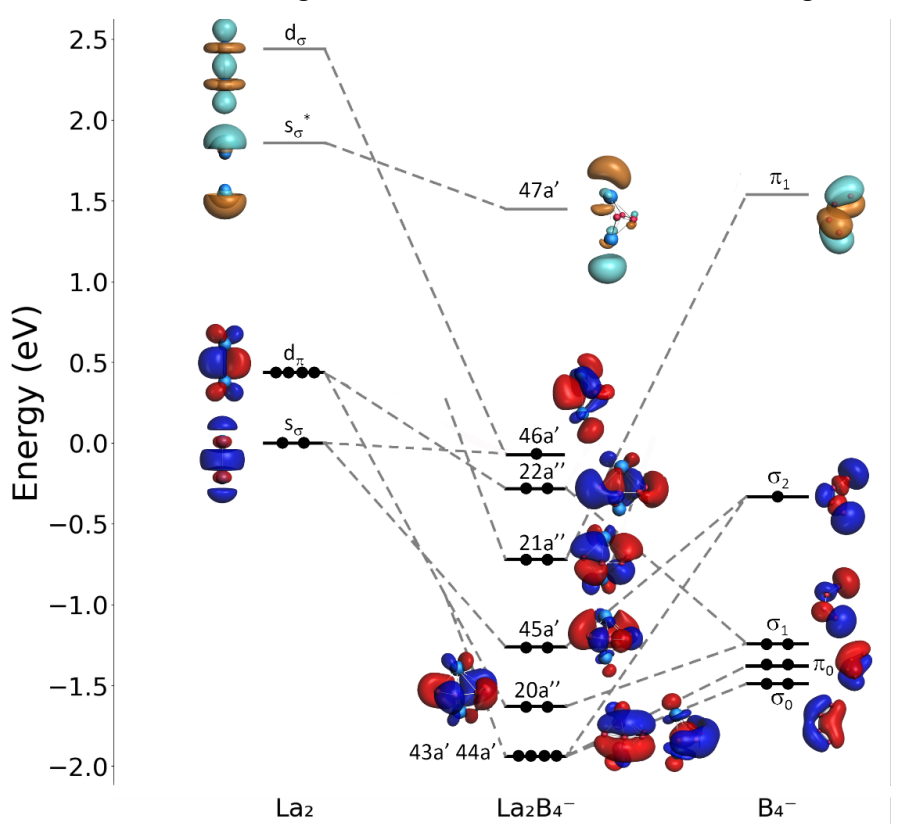


Figure 3. Correlation diagram between the molecular orbitals of La₂B₄ and those of the La₂ and B₄ fragments.

4.2. The Electronic Structure and La–La Bonding in La₂B_n⁻ (n = 4-6). We conducted MO analyses for La₂B₄⁻ as an example to understand the electronic structure and bonding mechanisms in the La₂B_n⁻

systems, as depicted in Figure 3. The analyses utilized the La₂ and B₄⁻ fragments, with the group orbitals of B₄⁻ labeled based on their shape and number of nodal planes. The 46a' HOMO mainly involves La–La bonding, primarily from the La s_{σ} and d_{σ} orbitals (72%, Table S2) with minor contributions from the B atoms. The antibonding La–La MO is the LUMO 47a' at an energy of 1.51 eV, indicating a large HOMO-LUMO gap in the anion. On the other hand, the energy separation between 46a' and 22a'' is relatively small, suggesting that filling another electron in the 46a' orbital would yield an electronically stable La₂B₄²⁻ system with a full La–La σ bond (*vide infra*).

According to the EDA-NOCV analyses shown in Table S3, the La₂B₄⁻ cluster exhibits slight ionic character, with electrostatic interactions accounting for 53% of the sum of ΔE_{orb} and ΔE_{elest} . The most significant interaction originates from electron flow from La₂ d_{π} to B₄⁻ π_1 , forming the 21a" orbital. The second most significant interaction arises from the 22a" orbital, with electron flow from La₂ d_{π} to B₄⁻ σ_1 . Additionally, using the La₂ ($s_{\sigma}^2 d_{\pi}^4$) fragment, we identified a NOCV orbital on the β spin channel with electron flow from La₂ d/s σ to the B₄ group orbital, where $\Delta \rho$ is 0.78. However, the corresponding α spin counterpart has negligible contributions, with only 0.8% to the total ΔE_{orb} , indicating that the singly occupied electron in La₂B₄⁻ primarily arises from La–La σ bonding with minimal contribution from La–B interactions. In La₂B₅⁻, however, strong La-B₅-La interactions involving the La 5*d* orbitals are observed, as demonstrated by the EDA-NOCV analyses (Table S4). Similar to the inverse-sandwich complexes La₂B_n⁻ (n = 7-9),¹¹⁻¹³ the dominant contribution arises from d-p-d π/δ interactions. The orbital corresponding to $\Delta E_{\text{orb}(4)}$ features La-B₅-La d-p-d σ bonding, in contrast to the La–La σ bonding observed in La₂B₄⁻. In the inverse sandwich complexes, the strong La-B_n-La interactions lead to increased 6*s*-6*s* repulsion, disfavoring efficient d/s hybridization necessary for La–La σ bonding.

In the global minimum structure of $La_2B_6^-$, we observed La–La σ bonding similar to that in $La_2B_4^-$, as illustrated in the 50a' orbital shown in Table S2. Unlike the inverse sandwich complexes without La–La bonding, the global minimum structure of $La_2B_6^-$ features one La atom within the B_6 plane forming a B_7 -like structure, ⁵⁰ which then forms a half-sandwich with the other La atom. This structure is a direct result of the high electronic stability of the B_7^{3-} borozene. ^{19,29} Most interestingly, there is direct La–La σ bonding in this structure, with a large bond order of 1.01 from the Gopinathan-Jug method ⁵⁹ and 1.06 from the Nalewajski-Mrozek (N-M) method, ⁶⁰⁻⁶² as shown in Table S5.

4.3. AdNDP Bonding Analyses for La₂B_n⁻ (n = 4-6). The chemical bonding in La₂B_n⁻ (n = 4-6) is further analyzed using the AdNDP method. Due to the open-shell nature of La₂B₄⁻, it is more convenient to add an electron into the La–La bonding HOMO (46a') to make the closed-shell La₂B₄²⁻. We optimized

the geometry of La₂B₄²⁻, which shows only a very slight distortion from the C_s symmetry of La₂B₄⁻ while maintaining the fully occupied La–La σ bonding MO. The AdNDP analyses for La₂B₄²⁻ presented in Figure 4 reveal three 2c-2e B–B σ bonds and a 2c-2e La–La σ bond. Two additional 2c-2e La–B σ bonds were identified between one La atom and its neighboring two B atoms. Consequently, this La atom acts as a "pseudo-B," forming a 5-membered ring, consistent with the C_s La₂B₄⁻ structure showing one La atom has two shorter La–B bonds (2.53 Å in Figure 2). The remaining delocalized orbitals consist of two 6c-2e σ bonds and two 6c-2e π bonds, involving chemical bonding between the second La atom with the five-membered ring and forming a stable La₂B₄²⁻ cluster with a strong La–La bond.

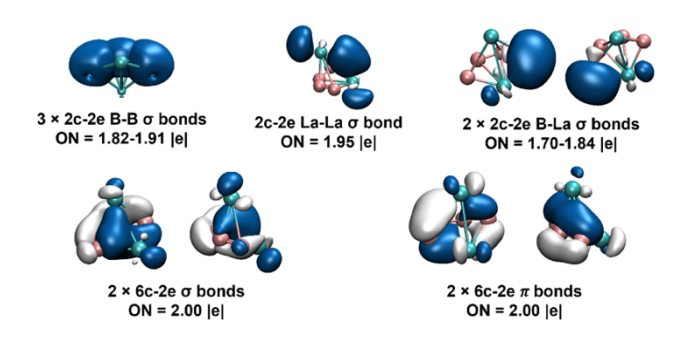


Figure 4. AdNDP bonding analyses for La₂B₄²⁻ at the PBE0/cc-pVTZ/ECP28MWB level.

The AdNDP analyses for La₂B₅⁻ shown in Figure 5 revealed four 2c-2e B–B σ bonds within the open B₅ ring and two 3c-2e La-B-La bonds involving both La atoms and the two terminal boron atoms. The remaining five bonds are all 7c-2e bonds involving interactions between the open B₅ ring and the two La atoms. These bonds are remarkably similar to those observed in the La₂B_n⁻ (n = 7-9) inverse sandwiches, ¹¹⁻¹³ suggesting that the C_{2v} La₂B₅⁻ cluster is an incomplete inverse-sandwich. This conclusion is supported by the fact that there is no La–La bond in La₂B₅⁻. The relatively short La–La distance in La₂B₅⁻ is a consequence of the strong La-B₅-La sandwich interactions, exactly the same as that in the La₂B_n⁻ (n = 7-9) inverse sandwiches.

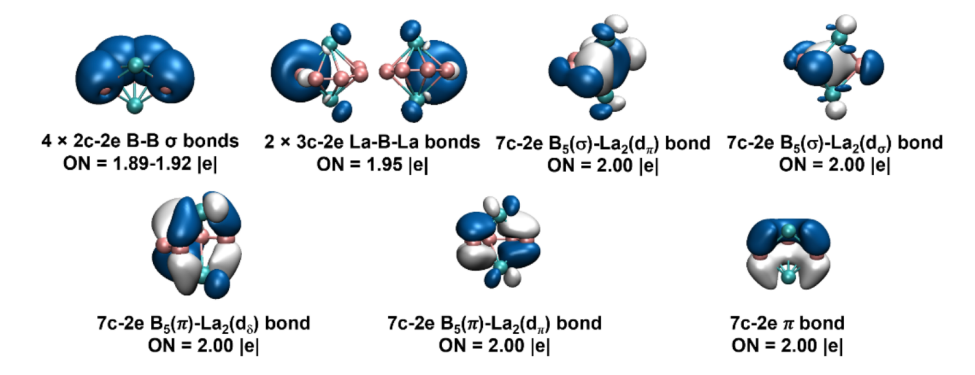


Figure 5. AdNDP bonding analyses for La₂B₅⁻ at the PBE0/cc-pVTZ/ECP28MWB level.

In the AdNDP analyses for La₂B₆⁻ (Figure 6), we observed one 2c-1e La–La σ bond, four 2c-2e peripheral B–B σ bonds, and two 2c-2e La–B σ bonds. Most interestingly, the three 8c-2e σ bonds and the three 8c-2e π bonds are reminiscent of the doubly aromatic bonding in the B₇³⁻ borozene. ^{19,29} This observation suggests that one of the La atom substitutes one B atom in B₇³⁻ to form a [LaB₆]³⁻ lanthaborozene. Thus, removing the electron from the HOMO of La₂B₆⁻ leads to the closed-shell neutral La₂B₆, which can be viewed as a lanthanide lanthaborozene complex, [La³⁺][LaB₆³⁻] (Figure S4a), similar to the [Pr³⁺][B₇³⁻] borozene complex reported previously. ¹⁵ However, the photoelectron spectrum of PrB₇⁻ revealed a large HOMO-LUMO gap of ~1.5 eV, suggesting that the neutral PrB₇ borozene complex is a much more stable electronic system. On the other hand, the LUMO of La₂B₆ is the La–La bonding orbital (50a', Table S2) and PES did not reveal a large HOMO-LUMO gap (the LUMO feature is so close to the HOMO feature that it is not resolved in band X in Figure 1c). Our calculation indicates a HOMO-LUMO gap of ~0.4 eV. Thus, filling the 50a' La–La bonding orbital will result in a stable [La₂B₆]²⁻ borozene complex with a La–La σ bond, as shown in the AdNDP analysis in Figure S4c.

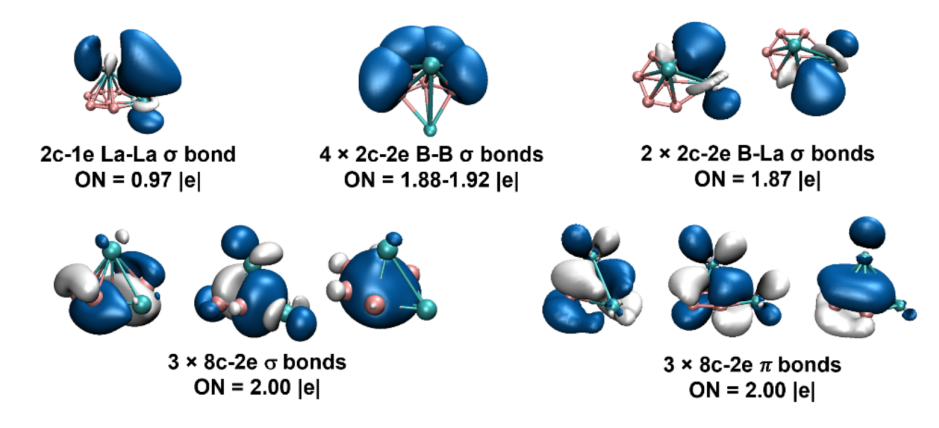


Figure 6. AdNDP bonding analyses for La₂B₆⁻ at the level of PBE0/cc-pVTZ/ECP28MWB level.

The La–La bonding in the La₂B_n⁻ (n = 4-6) clusters was further investigated using various bond order indices, as given in Table S5. The La–La bond order indices in La₂B₄⁻ and La₂B₆⁻ are found to be significantly larger than that in La₂B₅⁻. These results agree with the above bonding analyses, which reveal true La–La bonding in La₂B₄⁻ and La₂B₆⁻. On the other hand, there is no true La–La bonding in the incomplete inverse sandwich La₂B₅⁻, where the relatively short La–La distance is a result of strong La-B₅-La sandwich interactions. It should also be noted that the La–La bonding in the La₂B₄⁻ and La₂B₆⁻ clusters is reminiscent of the Ln–Ln bonding in the metallofullerenes¹ and the recently reported (Cp^{iPr5})₂Ln₂I₃ complexes,⁷ suggesting that lanthanide boride clusters afford an interesting platform to study Ln–Ln bonding.

5. CONCLUSIONS

In conclusion, we report an investigation of a series of di-lanthanum boron clusters, $La_2B_n^-$ (n=4-6), using photoelectron spectroscopy and ab initio quantum chemistry calculations. Global minimum searches revealed that $La_2B_4^-$ and $La_2B_5^-$ adopt incomplete B_4 and B_5 rings, respectively, sandwiched by two La atoms. While there is La-La bonding in $La_2B_4^-$, the bonding in $La_2B_5^-$ is similar to that in the larger inverse sandwich clusters, $La_2B_n^-$ (n=7-9), with no real La-La bonding. The global minimum of $La_2B_6^-$ departs from the growth path toward inverse sandwiches. Instead, one of the La atom can be viewed as substituting a B atom in the B_7^{3-} borozene to form a $[LaB_6]^{3-}$ lanthaborozene and the $La_2B_6^-$ cluster can be considered as a lanthanide lanthaborozene complex, $La^{2+}[LaB_6^{3-}]$ with La-La bonding. In both $La_2B_4^{2-}$ and $La_2B_6^{2-}$, a true two-electron La-La σ bond is found from the hybridized 6s5d orbitals. Lanthanide-lanthanide bonding is uncommom and Ln-B binary clusters provide excellent systems to search for and understand Ln-Ln bonding.

ASSOCIATED CONTENT

Supporting Information

The Supporting Information is available free of charge at https://pubs.acs.org/doi.10.1021/acs.inorchem.xxx. Low-lying isomers for $La_2B_n^-$ (n=4-6), AdNDP bonding analyses for $La_2B_6^{0/-/2-}$, coordinates of the global minimum structures of $La_2B_n^-$ (n=4-6), molecular orbitals and their compositions for $La_2B_n^-$ (n=4-6), EDANOCV analyses for $La_2B_4^-$ and $La_2B_5^-$, the La-La bond order indices in $La_2B_n^-$ (n=4-6) (PDF).

AUTHOR INFORMATION

Corresponding Authors

Teng-Teng Chen – Department of Chemistry, The Hong Kong University of Science and Technology, Clear Water Bay, Kowloon, Hong Kong (SAR) 999077 (China); HKUST Shenzhen-Hong Kong Collaborative Innovation Research Institute, Shenzhen 518045, China; orcid.org/0000-0001-9480-615X; Email: tengtengchen@ust.hk

Wan-Lu Li – Aiiso Yufeng Li Family Department of Chemical and Nano Engineering, University of California San Diego, CA 92093, United States; Program of Materials Science and Engineering, University of California San Diego, CA 92093, United States; orcid.org/0000-0003-0098-0670; Email: wal019@ucsd.edu

Lai-Sheng Wang – Department of Chemistry, Brown University, Providence, Rhode Island 02912, United States; orcid.org/0000-0003-1816-5738; Email: lai-sheng wang@brown.edu

Authors

Jordan Burkhardt – Aiiso Yufeng Li Family Department of Chemical and Nano Engineering, University of California San Diego, CA 92093, United States

Wei-Jia Chen – Department of Chemistry, Brown University, Providence, Rhode Island 02912, United States

Dao-Fu Yuan – Department of Chemistry, Brown University, Providence, Rhode Island 02912, United States; Hefei National Research Center for Physical Science at Microscale, University of Science and Technology of China, Hefei 230026, China

Author Contributions

[#]J. B. and T.T.C. contributed equally to this work.

Notes

The authors declare no competing financial interest.

ACKNOWLEDGEMENTS

The calculations were performed using the Expanse supercomputer at the San Diego Supercomputer Center (SDSC), through allocations of CHM230035 and CHE230113. W.L.L acknowledges startup funding from the Jacob School of Engineering at UCSD. The experiment done at Brown University was supported by the National Science Foundation (CHE-2403841). This work was supported in part by the Project of Hetao Shenzhen-Hong Kong Science and Technology Innovation Cooperation Zone (HZQB-KCZYB-2020083) and Young Elite Scientists Sponsorship Program by the Chinese Association of Science and Technology (CAST) (2023QNRC001).

References

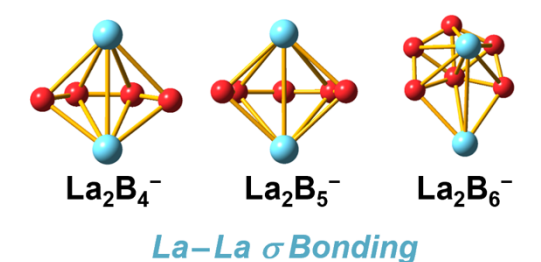
- (1) Liu, F.; Spree, L.; Krylov, D. S.; Velkos, G.; Avdoshenko, S. M.; Popov, A. A. Single-Electron Lanthanide-Lanthanide Bonds Inside Fullerenes toward Robust Redox-Active Molecular Magnets. *Acc. Chem. Res.* **2019**, *52*, 2981-2993.
- (2) Iiduka, Y.; Ikenaga, O.; Sakuraba, A.; Wakahara, T.; Tsuchiya, T.; Maeda, Y.; Nakahodo, T.; Akasaka, T.; Kako, M.; Mizorogi, N.; Nagase, S. Chemical Reactivity of Sc₃N@C₈₀ and La₂@C₈₀. *J. Am. Chem. Soc.* **2005**, *127*, 9956-9957.
 - (3) Kato, T. Metal Dimer and Trimer within Spherical Carbon Cage. J. Mol. Struct. 2007, 838, 84-88.
- (4) Lu, X.; Nikawa, H.; Nakahodo, T.; Tsuchiya, T.; Ishitsuka, M. O.; Maeda, Y.; Akasaka, T.; Toki, M.; Sawa, H.; Slanina, Z.; Mizorogi, N.; Nagase, S. Chemical Understanding of a Non-IPR Metallofullerene: Stabilization of Encaged Metals on Fused-Pentagon Bonds in La₂@C₇₂. *J. Am. Chem. Soc.* **2008**, *130*, 9129-9136.
- (5) Popov, A. A.; Avdoshenko, S. M.; Pendás, A. M.; Dunsch, L. Bonding between Strongly Repulsive Metal Atoms: An Oxymoron Made Real in a Confined Space of Endohedral Metallofullerenes. *Chem. Commun.* **2012**, *48*, 8031-8050.
- (6) Bao, L.; Chen, M.; Pan, C.; Yamaguchi, T.; Kato, T.; Olmstead, M. M.; Balch, A. L.; Akasaka, T.; Lu, X. Crystallographic Evidence for Direct Metal–Metal Bonding in a Stable Open-Shell La₂@I_h-C₈₀ Derivative. *Angew. Chem. Int. Ed.* **2016**, *55*, 4242-4246.
- (7) Gould, C. A.; McClain, K. R.; Reta, D.; Kragskow, J. G. C.; Marchiori, D. A.; Lachman, E.; Choi, E.-S.; Analytis, J. G.; Britt, R. D.; Chilton, N. F.; Harvey, B. G.; Long, J. R. Ultrahard Magnetism from Mixed-Valence Dilanthanide Complexes with Metal-Metal Bonding. *Science* **2022**, *375*, 198-202.

- (8) Ivanov, A. S.; Zhang, X.; Wang, H.; Boldyrev, A. I.; Gantefoer, G.; Bowen, K. H.; I. Cernusak, I. Anion Photoelectron Spectroscopy and CASSCF/CASPT2/RASSI Study of La_n^- (n = 1, 3-7). *J. Phys. Chem. A* **2015**, *119*, 11293–11303.
- (9) Kafader, J. O.; Topolski, J. E.; Jarrold, C. C. Molecular and Electronic Structures of Cerium and Cerium Suboxide Clusters. *J. Chem. Phys.* **2016**, *145*, 154306.
- (10) Huizenga, C.; Hratchian, H. P.; Jarrold, C. C. Lanthanide Oxides: From Diatomics to High-Spin, Strongly Correlated Homo- and Heterometallic Clusters. *J. Phys. Chem. A* **2021**, *125*, 6315–6331.
- (11) Li, W. L.; Chen, T. T.; Xing, D. H.; Chen, X.; Li, J.; Wang, L. S. Observation of Highly Stable and Symmetric Lanthanide Ccta-Boron Inverse Sandwich Complexes. *Proc. Natl. Acad. Sci. USA.* **2018**, *115*, E6972-E6977.
- (12) Chen, T. T.; Li, W. L.; Li, J.; Wang, L. S. $[La(\eta^x-B_x)La]^-$ (x = 7-9): A New Class of Inverse Sandwich Complexes. *Chem. Sci.* **2019**, *10*, 2534-2542.
- (13) Li, W. L.; Chen, T. T.; Jiang, Z. Y.; Wang, L. S.; Li, J. Recent Progresses in the Investigation of Rare-Earth Boron Inverse Sandwich Clusters. *Chinese J. Struc. Chem.* **2020**, *39*, 1009-1018.
- (14) Jiang, Z. Y.; Chen, T. T.; Chen, W. J.; Li, W. L.; Li, J.; Wang, L. S. Expanded Inverse-Sandwich Complexes of Lanthanum Borides: La₂B₁₀⁻ and La₂B₁₁⁻. *J. Phys. Chem. A* **2021**, *125*, 2622-2630.
- (15) Chen, T. T.; Li, W. L.; Jian, T.; Chen, X.; Li, J.; Wang, L. S. PrB_7^- : A Praseodymium-Doped Boron Cluster with a Pr^{II} Center Coordinated by a Doubly Aromatic Planar η^7 - B_7^{3-} Ligand. *Angew. Chem. Int. Ed.* **2017**, *56*, 6916-6920.
- (16) Robinson, P. J.; Zhang, X.; McQueen, T.; Bowen, K. H.; Alexandrova, A. N. SmB₆⁻ Cluster Anion: Covalency Involving f Orbitals. J. Phys. Chem. A **2017**, 121, 1849–1854.
- (17) Chen, X.; Chen, T. T.; Li, W. L.; Lu, J. B.; Zhao, L. J.; Jian, T.; Hu, H. S.; Wang, L. S.; Li, J. Lanthanide with Unusually Low Oxidation States in the PrB₃⁻ and PrB₄⁻ Boride Clusters. *Inorg. Chem.* **2019**, 58, 411-418.
- (18) Mason, J. L.; Harb, H.; Huizenga, C. D.; Ewigleben, J. C.; Topolski, J. E.; Hratchian, H. P.; Jarrold, C. C. Electronic and Molecular Structures of the CeB₆ Monomer. *J. Phys. Chem. A* **2019**, *123*, 2040–2048.
- (19) Li, W. L.; Chen, T. T.; Chen, W. J.; Li, J.; Wang, L. S. Monovalent Lanthanide(I) in Borozene Complexes. *Nat. Commun.* **2021**, *12*, 6467.
- (20) Wang, Z. L.; Chen, T. T.; Chen, W. J.; Li, W. L.; Zhao, J.; Jiang, X. L.; Li, J.; Wang, L. S.; Hu, H. S. The Smallest 4f-Metalla-Aromatic Molecule of Cyclo-PrB₂⁻ with Pr–B Multiple Bonds. *Chem. Sci.* **2022**, *13*, 10082-10094.
- (21) Jin, S.; Sun, W.; Chen, B.; Kuang, X.; Lu, H.; Lu, C. Insights into the Structures and Bonding of Medium-Sized Cerium-Doped Boron Clusters. *J. Phys. Chem. A* **2021**, *125*, 4126–4132.
- (22) Chen, B.; Gutsev, G. L.; Dengfeng Li, D.; Ding, K. Structure and Chemical Bonding in Medium-Size Boron Clusters Doped with Praseodymium. *Inorg. Chem.* **2022**, *61*, 7890–7896.
- (23) Chen, T. T.; Li, W. L.; Chen, W. J.; Li, J.; Wang, L. S. La₃B₁₄⁻: An Inverse Triple-Decker Lanthanide Boron Cluster. *Chem. Commun.* **2019**, *55*, 7864-7867.
- (24) Chen, T. T.; Li, W. L.; Chen, W. J.; Yu, X. H.; Dong, X. R.; Li, J.; Wang, L. S. Spherical Trihedral Metallo-Borospherenes. *Nature Commun.* **2020**, *11*, 2766.
- (25) Li, W. L.; Ertural, C.; Bogdanovski, D.; Li, J.; Dronskowski, R. Chemical Bonding of Crystalline LnB₆ (Ln = La–Lu) and Its Relationship with Ln₂B₈ Gas-Phase Complexes. *Inorg. Chem.* **2018**, *57*, 12999-13008.
- (26) Scheifers, J. P.; Zhang, Y.; Fokwa, B. P. T. Boron: Enabling Exciting Metal-Rich Structures and Magnetic Properties. *Acc. Chem. Res.* **2017**, *50*, 2317–2325.
- (27) Munarriz, J.; Robinson, P. J.; Alexandrova, A. N. Towards a Single Chemical Model for Understanding Lanthanide Hexaborides. *Angew. Chem. Int. Ed.* **2020**, *59*, 22684–22689.

- (28) Ndiaye, S.; Bhorade, O.; Blum, I.; Klaes, B.; Bacchi, C.; Houard, J.; Vella, A.; Vurpillot, F.; Rigutti, L. Isotopic Correction of Compositional Inaccuracies in the Atom Probe Analysis of LaB₆. *J. Phys. Chem. C* **2024**, *128*, 2937-2947.
- (29) Wang, L. S. Borozenes: Benzene-Like Planar Aromatic Boron Clusters. *Acc. Chem. Res.* **2024**, online. https://pubs.acs.org/doi/full/10.1021/acs.accounts.4c00380.
- (30) Wang, L. S. Photoelectron Spectroscopy of Size-Selected Boron Clusters: From Planar Structures to Borophenes and Borospherenes. *Int. Rev. Phys.* **2016**, *35*, 69-142.
 - (31) https://github.com/WanluLigroupUCSD/SDGMS.
- (32) ADF, 2024.1, SCM, Theoretical Chemistry, Vrijie Universiteit, Amsterdam, The Netherlands, (http://www.scm.com).
- (33) te Velde, G.; Bickelhaupt, F. M.; Baerends, E. J.; Fonseca Guerra, C.; van Gisbergen, S. J. A.; Snijders, J. G.; Ziegler, T. Chemistry with ADF. *J. Comput. Chem.* **2001**, *22*, 931-967.
- (34) Lenthe, E. v.; Baerends, E. J.; Snijders, J. G. Relativistic Total Energy Using Regular Approximations. *J. Chem. Phys.* **1994**, *101*, 9783-9792.
- (35) Louwerse, M. J.; Rothenberg, G. Transferable Basis Sets of Numerical Atomic Orbitals. *Phys. Rev. B* **2012**, *85*, 035108.
- (36) Perdew, J. P.; Burke, K.; Ernzerhof, M. Generalized Gradient Approximation Made Simple. *Phys. Rev. Lett.* **1996,** 77, 3865-3868.
- (37) Neese, F.; Wennmohs, F.; Becker, U.; Riplinger, C. The ORCA Quantum Chemistry Program Package. *J. Chem. Phys.* **2020**, *152*, 224108.
- (38) Neese, F. Software Update: The ORCA Program System—Version 5.0. WIREs Comp. Mol. Sci. 2022, 12, e1606.
 - (39) Li, J.; Li, X.; Zhai, H. J.; Wang, L. S. Au₂₀: A Tetrahedral Cluster. Science 2003, 299, 864-867.
- (40) Schipper, P. R. T.; Gritsenko, O. V.; Gisbergen, S. J. A. v.; Baerends, E. J. Molecular Calculations of Excitation Energies and (Hyper)polarizabilities with a Statistical Average of Orbital Model Exchange-Correlation Potentials. *J. Chem. Phys.* **2000**, *112*, 1344-1352.
- (41) Zubarev, D. Y.; Boldyrev, A. I. Developing Paradigms of Chemical Bonding: Adaptive Natural Density Partitioning. *Phys. Chem. Chem. Phys.* **2008**, *10*, 5207-5217.
- (42) Frisch, M. J.; Trucks, G. W.; Schlegel, H. B.; Scuseria, G. E.; Robb, M. A.; Cheeseman, J. R.; Scalmani, G.; Barone, V.; Petersson, G. A.; Nakatsuji, H.; Li, X.; Caricato, M.; Marenich, A. V.; Bloino, J.; Janesko, B. G.; Gomperts, R.; Mennucci, B.; Hratchian, H. P.; Ortiz, J. V.; Izmaylov, A. F.; Sonnenberg, J. L.; Williams; Ding, F.; Lipparini, F.; Egidi, F.; Goings, J.; Peng, B.; Petrone, A.; Henderson, T.; Ranasinghe, D.; Zakrzewski, V. G.; Gao, J.; Rega, N.; Zheng, G.; Liang, W.; Hada, M.; Ehara, M.; Toyota, K.; Fukuda, R.; Hasegawa, J.; Ishida, M.; Nakajima, T.; Honda, Y.; Kitao, O.; Nakai, H.; Vreven, T.; Throssell, K.; Montgomery Jr., J. A.; Peralta, J. E.; Ogliaro, F.; Bearpark, M. J.; Heyd, J. J.; Brothers, E. N.; Kudin, K. N.; Staroverov, V. N.; Keith, T. A.; Kobayashi, R.; Normand, J.; Raghavachari, K.; Rendell, A. P.; Burant, J. C.; Iyengar, S. S.; Tomasi, J.; Cossi, M.; Millam, J. M.; Klene, M.; Adamo, C.; Cammi, R.; Ochterski, J. W.; Martin, R. L.; Morokuma, K.; Farkas, O.; Foresman, J. B.; Fox, D. J. Gaussian 16 Rev. C.01, Wallingford, CT, 2016.
- (43) Cao, X.; Dolg, M. Valence Basis Sets for Relativistic Energy-Consistent Small-Core Lanthanide Pseudopotentials. *J. Chem. Phys.* **2001**, *115*, 7348-7355.
- (44) Cao, X.; Dolg, M. Segmented Contraction Scheme for Small-Core Lanthanide Pseudopotential Basis Sets. *J. Mol. Struct.* **2002**, *581*, 139-147.

- (45) Dunning Jr, T. H. Gaussian Basis Sets for Use in Correlated Molecular Calculations. I. The Atoms Boron through Neon and Hydrogen. *J. Chem. Phys.* **1989**, *90*, 1007-1023.
- (46) Kendall, R. A.; Dunning, T. H., Jr.; Harrison, R. J. Electron Affinities of the First-Row Atoms Revisited. Systematic Basis Sets and Wave Functions. *J. Chem. Phys.* **1992**, *96*, 6796-6806.
- (47) Woon, D. E.; Dunning, T. H., Jr. Gaussian Basis Sets for Use in Correlated Molecular Calculations. III. The Atoms Aluminum through Argon. *J. Chem. Phys.* **1993**, *98*, 1358-1371.
- (48) Michalak, A.; Mitoraj, M.; Ziegler, T. Bond Orbitals from Chemical Valence Theory. *J. Phys. Chem. A* **2008**, *112*, 1933-1939.
- (49) Mitoraj, M. P.; Michalak, A.; Ziegler, T. A Combined Charge and Energy Decomposition Scheme for Bond Analysis. *J. Chem. Theory Comput.* **2009**, *5*, 962-975.
- (50) Alexandrova, A. N.; Boldyrev, A. I.; Zhai, H. J.; Wang, L. S. Electronic Structure, Isomerism, and Chemical Bonding in B₇ and B₇. *J. Phys. Chem.* A **2004**, *108*, 3509-3517.
- (51) Romanescu, C.; Sergeeva, A. P.; Li, W. L.; Boldyrev, A. I.; Wang, L. S. Planarization of B₇⁻ and B₁₂⁻ Clusters by Isoelectronic Substitution: AlB₆⁻ and AlB₁₁⁻. *J. Am. Chem. Soc.* **2011**, *133*, 8646-8653.
- (52) Barroso, J.; Sudip Pan, S.; Merino, G. Structural Transformations in Boron Clusters Induced by Metal Doping. *Chem. Soc. Rev.* **2022**, *51*, 1098–1123.
- (53) Li, W. L.; Ivanov, A. S.; Federic, J.; Romanescu, C.; Cernusak, I.; Boldyrev, A. I.; Wang, L. S. On the Way to the Highest Coordination Number in the Planar Metal-Centered Aromatic $Ta@B_{10}^-$ Cluster: Evolution of the Structures of TaB_n^- (n = 3-8). *J. Chem. Phys.* **2013**, *139*, 104312.
- (54) Cheung, L. F.; Czekner, J.; Kocheril, G. S.; Wang, L. S. ReB₆⁻: A Metallaboron Analog of Metallabenzenes. *J. Am. Chem. Soc.* **2019**, *141*, 17854-17860.
- (55) Cheung, L. F.; Kocheril, G. S.; Czekner, J.; Wang, L. S. MnB₆⁻: An Open-Shell Metallaboron Analog of 3d Metallabenzenes. *J. Phys. Chem. A* **2020**, *124*, 2820-2825.
- (56) Xie, L.; Li, W.-L.; Romanescu, C.; Huang, X.; Wang, L. S. A Photoelectron Spectroscopy and Density Functional Study of Di-Tantalum Boride Clusters: $Ta_2B_x^-$ (x = 2-5). *J. Chem. Phys.* **2013**, *138*, 034308.
- (57) Li, W. L.; Xie, L.; Jian, T.; Romanescu, C.; Huang, X.; Wang, L. S. Hexagonal Bipyramidal $[Ta_2B_6]^{-/0}$ Clusters: B₆ Rings as Structural Motifs. *Angew. Chem. Int. Ed.* **2014**, *126*, 1312-1316.
- (58) Pyykkö, P. Additive Covalent Radii for Single-, Double-, and Triple-Bonded Molecules and Tetrahedrally Bonded Crystals: A Summary. *J. Phys. Chem. A* **2015**, *119*, 2326-2337.
- (59) Gopinathan, M. S.; Jug, K. Valency. I. A Quantum Chemical Definition and Properties. *Theor. Chim. Acta* **1983**, 63, 497-509.
- (60) Nalewajski, R. F.; Mrozek, J.; Michalak, A. Two-Electron Valence Indices from the Kohn-Sham Orbitals. *Int. J. Quantum Chem.* **1997**, *61*, 589-601.
- (61) Nalewajski, R. F.; Mrozek, J. Modified Valence Indices from the Two-Particle Density Matrix. *Int. J. Quantum Chem.* **1994**, *51*, 187-200.
- (62) Nalewajski, R. F.; Mrozek, J.; Mazur, G. Quantum Chemical Valence Indices from the One-Determinantal Difference Approach. *Can. J. Chem.* **1996**, *74*, 1121-1130.

ToC graphic:



The structures and bonding of a series of di-lanthanum boron clusters, $La_2B_n^-$ (n = 4-6), are investigated both experimentally and theoretically. The structures of $La_2B_4^-$ and $La_2B_5^-$ are found to adopt incomplete B_4 and B_5 rings, whereas one La atom in $La_2B_6^-$ is found to be part of the B_6 plane and can be viewed as substituting one B atom in a B_7 cluster. La-La σ bond is found in $La_2B_4^-$ and $La_2B_6^-$.